Natural Resources Research, Vol. 30, No. 1, February 2021 (© 2020)
https://doi.org/10.1007/s11053-020-09722-3

Original Paper

Determination of Reservoir Flow Units from Core Data: A Case Study of the Lower Cretaceous Sandstone Reservoirs, Western Bredasdorp Basin Offshore in South Africa

Mimonitu Opuwari,[1,2] Saeed Mohammed,[1] and Charlene Ile[1]

Received 25 April 2020; accepted 8 July 2020
Published online: 21 July 2020

The overarching aim of this study is to use core measurements of porosity and permeability in three wells (MO1, MO2, and MO3) to generate a scheme of sandstone reservoir zonation for identification of flow units in the E-M gas field of the Western Bredasdorp Basin Offshore in South Africa. The evaluation method began by establishing rock types within a geological framework that allowed the definition of five facies, grouped as facies A, B, C, D, and E. Facies A was recognized as the best petrophysical rock type. In contrast, facies E was recognized as impervious rock. The results of independent reservoir classification methods were integrated to identify flow zones that yielded positive results. The results ultimately culminated in a zonation scheme for the Basin. Twelve flow zones were identified and were broadly classified as high, moderate, low, very low, and tight zones. The high zone was characterized by pore throat radius of ≥ 10 μm, flow zone index (FZI) of ≥ 5.0 μm, and flow unit efficiency (FUE) of ≥ 0.8. In contrast, very low efficiency zones had pore throat radius and FZI of < 2 μm, and FUE of ≤ 0.2. The high-efficiency zones were comparable to facies A and the tight zone to facies E. Facie C provided sand–sand contacts that allowed flow between the zones. One high, two moderate, four low, and five very low efficiency zones were identified. The plot of FUE can be compared directly with flowmeter logs. The results obtained from this study will serve as an input parameter for reservoir studies in the western Bredasdorp Basin.

KEY WORDS: Flow unit efficiency, Pore throat radius, Hydraulic flow units, Bredasdorp Basin, Lorentz plot.

INTRODUCTION

The target reservoirs of this study are the sandstone reservoirs deposited in Valanginian of Lower Cretaceous. They comprise three exploration wells (MO1, MO2, and MO3) of the E-M gas field in the western part of the western Bredasdorp Basin (Fig. 1), which is a sub-basin of the Outeniqua Basin, located at South Africa's southernmost continental boundary. The western Bredasdorp Basin has an aerial extent of about 18,000 km^2, which begins off the southeast coast of Cape Town and stretches up the southeast coast, until Port Elizabeth (Wood 1995). The western Bredasdorp Basin emanated from extensional episodes during the early stages of rifting in middle to late Jurassic (Roux 2000; Broad et al. 2006).

For accurate predictive petrophysical rock classification from well logs, it is essential to study

[1]Petroleum Geosciences Research Group, Department of Earth Sciences, University of the Western Cape, Cape Town, South Africa.
[2]To whom correspondence should be addressed; e-mail: mopuwari@uwc.ac.za

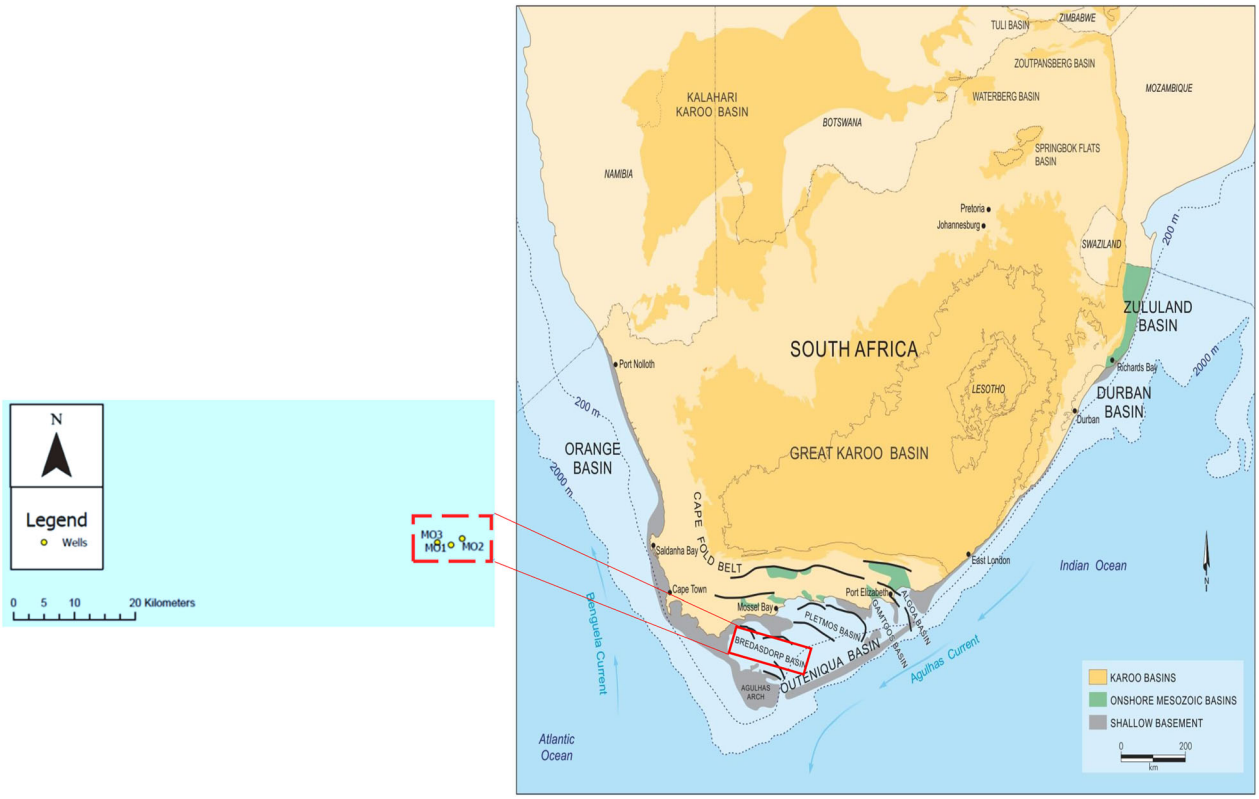

Figure 1. Map showing the study area location offshore in South Africa. (Petroleum Agency of South Africa 2003).

thoroughly the rock types and their petrophysical variabilities from core data as a means to guide log-based classification (Xu et al. 2012). One of the most important targets of core studies is to calibrate log data; that is why core data are regarded as ground truth in reservoir study. The recognition of reservoir quality is essential in reservoir characterization, as it describes a reservoir's storage capacity, which is a function of porosity and venerability, which in turn are a function of permeability (El Sharawy and Nabawy 2019).

The assembly of reservoir rocks into hydraulic units (HUs) is achieved by the relationship between permeability and porosity, as initially proposed by Carman (1937). Flow units (FUs) were initially described as representing larger scale corresponding units between wells (Ebanks 1987). A reservoir FU is a stratigraphically continuous interval of similar reservoir process efficiency that maintains the geological framework and the characteristics of rock types with distinct porosity and permeability relationship (Gunter et al. 1997). A FU is mostly controlled by prevalent depositional properties and the diagenetic history as well as the petrophysical properties (Nabawy and Geraud 2016).

Various definitions of rock typing and petrophysical rock units have been suggested in the literature for both geological and petrophysical rock units (Corbett and Potter 2004). Hydraulic flow units (HFUs) in reservoirs have been determined by various traditional methods in several case studies in carbonate as well as sandstone reservoirs (e.g., Hearn et al. 1984; Slatt and Hopkins 1990; Grier and Marschall 1992; Pittman 1992; Amaefule et al. 1993; Ellabad et al. 2001; Uguru et al. 2005; Bhattacharya et al. 2008; Chekani and Kharrat 2009; Aguilera 2014; Abuseda et al. 2015; Nabawy and Al-Azazi 2015; Moradi et al. 2017; Mirzaei-Paiaman et al. 2018; Riazi 2018; Zhang et al. 2018;El Sharawy and Nabawy 2019). However, there is a paucity of published work on the sandstone reservoirs in the western Bredasdorp Basin. Some of published work on reservoir characterization and formation evaluation of the western Bredasdorp Basin includes,

among others, those of Ojongokpoko (2006), Hussien (2014), Acho (2015), Maseko (2016), and Magoba and Opuwari (2017).

This study aimed to provide new insights into the identification of FUs for reservoir studies and the simulation for the western Bredasdorp Basin. This is part of ongoing research to identify intervals within sandstone reservoirs that contribute optimally to the flow and to identify similar intervals in other parts of the western Bredasdorp Basin. This would culminate in the creation of a scheme for effective zonation. The initial process of core data investigation started with the grouping of core facies in order to understand the relationship between facies and petrophysical rock units. The knowledge of this relationship is essential because, in clastic reservoirs, HUs are controlled by their primary depositional textures and their diagenetic history (Stonecipher et al. 1984; Corbett et al. 2001; Cerepi et al. 2003; Tavakoli et al. 2011).

The two graphical methods used in this study to determine FUs from conventional core porosity and permeability values were (1) HU and (2) FU. The hydraulic methods used were the Winland r35 and the reservoir quality index (RQI) of Amaefule et al. (1993). The FU method used is the stratigraphic modified Lorenz plot (SMLP) and the flow unit efficiency (FUE) method. The FU method differs from the HU method in that they are bounded by significant changes in permeability although HUs are bounded by barriers to vertical a flow (Shepherd 2009). These methods were applied in three wells (MO1, MO2, and MO3), for which a conventional gamma-ray log as well as core porosity and permeability data were available. The results of a flow zonation scheme were then applied to identify flow zones/units.

LOCATION AND GEOLOGY OF THE STUDY AREA

Deep marine sedimentation, faults, and widespread development of red and green claystones, overlaid by porous glauconitic littoral sandstones, are common features in the Basin (McMillan et al. 1997), which resulted in the creation of essential elements of a petroleum system. An exploration of the deep and ultra-deep waters off South Africa's coast is ongoing, and the recently acquired exploration data are yielding new insights into the formation and the depositional environments of sediments within the Basin (Selley and Van der Spuy 2016).

Sandstone reservoirs in the western Bredasdorp Basin comprise stacked and amalgamated channels and fan lobes that have been described as coarsening upwards, while fining upward cycles are in channelized reservoirs (Turner et al. 2000). There are mainly two types of reservoir rocks found in the western Bredasdorp Basin, (a) rocks deposited in the shelf that are shallow marine to fluvial of the syn-rift section and (b) deep marine deposits in the drift section (Petroleum Agency of South Africa 2003).

The western Bredasdorp Basin infill is composed of sediments of Upper Jurassic and Early Cretaceous fluvial and shallow marine syn-rift continental deposits, which consist of a complex pre-rift geological framework that has developed into two phases of the tectonic framework. The stratigraphic column reflects the development of the two phases, which are the syn-rift phase (late Jurassic and the Early Cretaceous), followed by the drift phase in the Early Cretaceous to Tertiary (Jungslager 1999; Petroleum Agency of South Africa 2003).

The syn-rift I phase deposits comprise four lithological units that resulted from major intercalated marine transgression and regression cycles. These lithological units include the lower fluvial interval, which represents an initial graben fill comprising claystones, sandstones, and conglomerates deposited as alluvial fans in fluvial environments. The second lithological unit is a lower shallow marine interval unit indicating the first marine incursion into the Basin, which is composed of glauconitic and fossiliferous sandstones. The third unit is the Upper Fluvial interval characterized by an alluvial floodplain and meandering fluvial deposits. In contrast, the fourth unit is the upper shallow marine interval characterized by massive glauconitic and fossiliferous sandstones of Late Valanginian age, deposited as transgressive beach facies (Broad et al. 2006).

The syn-rift II phase occurred during the Late Valanginian to the Hauterivian and were marked by the 1At1 to the 6At1 sequence boundary, referred to as a renewed rifting phase indicated by the 1At1 unconformity (Jungslager 1999). The rapid subsidence and the extensive flooding distinguish syn-rift II.

The transitional period, which is in the early drift phase, occurred after syn-rift II during the Hauterivian to the Aptian. It indicates change from

a passive margin to a transform margin (Ngejane 2014). The drift phase occurred during the Albian and continued to the present day (Davies 1997). The drift phase is marked by the 14At1 unconformity, which recorded the beginning of the onset of thermally induced subsidence and eustatic effects. All the mentioned features as well as the standard chronostratigraphy of the western Bredasdorp Basin are based on the results of sequence stratigraphy (Brown et al. 1996; Jungslager 1999; Elliott 1997). A unique chronostratigraphic framework for the western Bredasdorp Basin is presented in Figure 2, showing the focus of the study on the lower Cretaceous shallow marine and fluvial sediments.

MATERIALS AND METHODS

For this study, the Petroleum Agency of South Africa (PASA) provided the conventional core data of 705 samples of porosity and permeability, as well as mineral composition and gamma-ray log data of three exploration wells (255 plugs from MO1, 232 plugs from MO2, and 232 plugs from MO3) in the western Bredasdorp Basin in South Africa. Data processing commenced with the creation of a database in a Microsoft Excel spreadsheet, where all the preliminary data quality checks, the preparations, and the calculation were conducted before loading all the data into an IP4.2 program. (Interactive petrophysics is a software program for the analysis and the interpretation of petrophysical data.) The classification of core facies was achieved by using the core description reports provided in conjunction with the petrophysical behaviors of rock units and the gamma-ray log pattern observations, to classify the lithology into five lithofacies. In this study, different petrophysical methods for core-based rock type classification were adopted to classify rock types based on core measurements.

The first method of HU used is the Winland 1972 method (Kolodzie 1980) because petrophysical rock classification considers both storage and flow capacity of reservoir rocks and should be based on both pore size distribution and connectivity (Archie 1950; Rushing et al. 2008; Xu et al. 2012). The Winland r35 plot is a semi-log cross-plot of permeability against porosity with an isopore line, which corresponds to a calculated pore throat radius of 35% of mercury saturation as mentioned by Winland (Kolodzie 1980). The pore throat radius (r) was calculated from core permeability and porosity data as follows (Kolodzie 1980; Pittman 1992; Gunter et al. 1997):

$$\log(r35\%) = 0.732 + 0.588\log(K_{\text{air}}) - 0.864\log(\Phi) \quad (1)$$

where r is pore throat radius (μm), K_{air} is air permeability (mD), and Φ is porosity (%).

The second method of HU used is the integration of a hydraulic concept (Amaefule et al. 1993) and the reservoir potential index (RPI) method (Nabawy and Al-Azazi 2015) for delineating reservoirs into distinct petrophysical rock units. Each unit has a unique RQI, a normalized porosity index (NPI), and a flow zone index (FZI), each calculated from core permeability and porosity data. This concept is based on the calculation of two terms, RQI and NPI, to determine the FZI, which is the HFU identifier following Amaefule et al. (1993) and the ranking of units by Nabawy and Al-Azazi (2015) and Nabawy et al. (2018), thus:

$$\text{RQI} = 0.0314 * \sqrt{K/\Phi} \quad (2)$$

$$\text{NPI} = \Phi/(1-\Phi) \quad (3)$$

$$\text{FZI} = \text{RQI}/\text{NPI} \quad (4)$$

$$\text{RPI} = (\text{RQI rank} + \text{FZI rank})/2 \quad (5)$$

where K is permeability (mD), Φ is porosity (v/v), RQI and FZI are ranks with of μm, and RPI is reservoir potential index, which is the arithmetic average of RQI and FZI ranks.

The first method of FU used was the SMLP (Gunter et al. 1997). The SMLP was used to identify storage and flow capacities of the reservoir based on core porosity, permeability and bed thickness. The method utilizes the computation of percentage flow capacity, which is the product of permeability, thickness, and percentage storage capacity. The derived values were then normalized, and cumulative storage and flow capacities were obtained. The cumulative percentage of flow vs. storage capacities were plotted to obtain a curve. The slope or the points of the inflexions were then interpreted preliminarily to represent various FU intervals, whether they are efficiency zones, baffle or barrier units (Chopra et al. 1987; Newsham and Rushing 2001; Gomes et al. 2008; Mahjour et al. 2016).

The second method of FU used was the FUE, which is the cumulative percentage of flow capacity divided by the cumulative percentage of storage

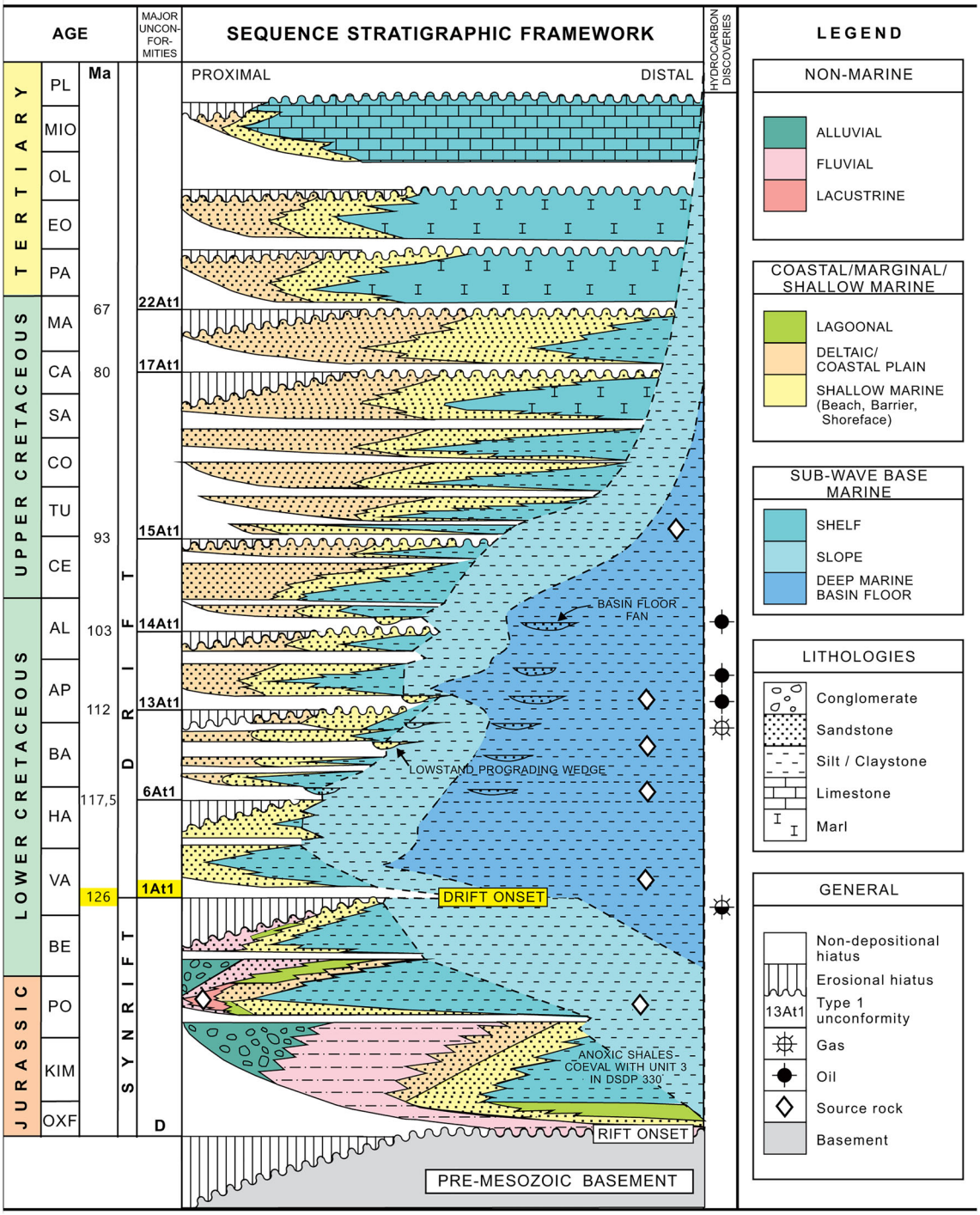

Figure 2. Chronostratigraphic and sequence chart showing major unconformities as well as possible source rock intervals (Jungslager 1999; Ramiah et al. 2019). Red rectangles indicate the area of study.

capacity, that separate FU zones into high, moderate, low, and very low units (Bhattacharya et al. 2008). The results from the classification of rock types using petrophysical methods are juxtaposed and integrated with facies, to develop a scheme of sandstone reservoir zonation to identify the flow zones.

RESULTS AND DISCUSSION

Core Description

The sediments evaluated are mainly from shallow marine and fluvial depositional environments, classified into five different facies. Facies were regarded as a distinctive body of rock that was formed under certain conditions of sedimentation, reflecting a particular process and a set of conditions (Reading 2001). The primary objective of describing the core samples in detail was to establish characteristic facies, based on the grain size, in each well. The integration of a previous sedimentology report with gamma-ray log signatures enabled the classification of the rock types into the following five different facies:

- **Facies A** Fine- to medium-grained sandstone with minor shales, moderately cemented.
- **Facies B** Fining upwards grained sandstones, pebbly toward the base, moderately sorted.
- **Facies C** Fine- to very fine-grained with variable argillaceous sandstones.
- **Facies D** Interbedded sandstones and shales, very fine sandstones with well-sorted grains, very well-cemented.
- **Facies E** Silty shale and bioturbated.

The gamma-ray log is a lithology indicator for siliciclastic environment (Eichkitz et al. 2009). Sandstones rich in potassium minerals such as potassium feldspar, muscovite mica, illite, and gluconate can give a high gamma-ray response that is easily mistaken for shale. The log shapes in gamma-ray logs are related to sediment character and depositional environment. Shapes in gamma-ray logs can be interpreted as grain size trends and, by sedimentological association, as cycles (Selley 1998; Rider and Rider 2002; Jipa 2012; Das and Chatterjee 2018). Therefore, the collaboration of a gamma-ray log response with core information makes interpretations more reliable.

The five facies were compared to the gamma-ray log response (Fig. 3a–c). By correlating the facies with the log shape response, we interpreted the reservoir as serrated due to variable sandstone, siltstone, and possible traces of potassium mineral. The GR value for facies A, which is a thick serrated sandstone with minor shale, ranged from 30 to 50 API, while facies B, which displays fining upward sequence in part, had GR values from 28 to 58 API. The gamma-ray value for facies C, D, and E displayed GR values of 58–76, 76–87, and 87–117 API, respectively.

Wells MO1 and MO2 displayed five facies, whereas for well MO3, three facies were observed (Fig. 3). In terms of reservoir quality, facies A represented the best petrophysical reservoir, followed by facies B, while facies C was of intermediate quality; facies D had poor quality, while facies E was considered an impervious reservoir rock type. Our interpretation is supported by Shepherd (2009) that a moderate volume of cement may not cause problems from reservoirs in thick, continuous sandstone intervals which is observed in facies A. The next step in the workflow was to analyze the petrophysical methods and to integrate the results with the facies.

Petrophysical Rock Type Determination by Winland r35 Method

A petrophysical rock type (PRT) determined from the Winland r35 method is regarded as an interval of rock with similar average pore throat radius and having similar fluid flow characteristics (Boada et al. 2001; Porras and Campos 2001). The characterization of rock type depends on the flow and storage capacities of a rock, using capillary pore throat distribution, porosity, and permeability measurements as inputs. Pore throat size may be determined from conventional core analysis of porosity and permeability data by using the Winland equation (Porras et al. 1999). In this study, four PRTs were identified from the results of the Winland r35 pore throat determination based on core porosity (Phi), permeability (k) and k/Phi ratio. Table 1 summarizes the variability associated with petrophysical properties associated with each rock type, while Figure 4 indicates distinct trends of porosity and permeability per rock type. The rock quality was characterized using the Winland r35 calculated values with diagonal curve lines representing equal r35 values. Data points that plot along a constant ratio

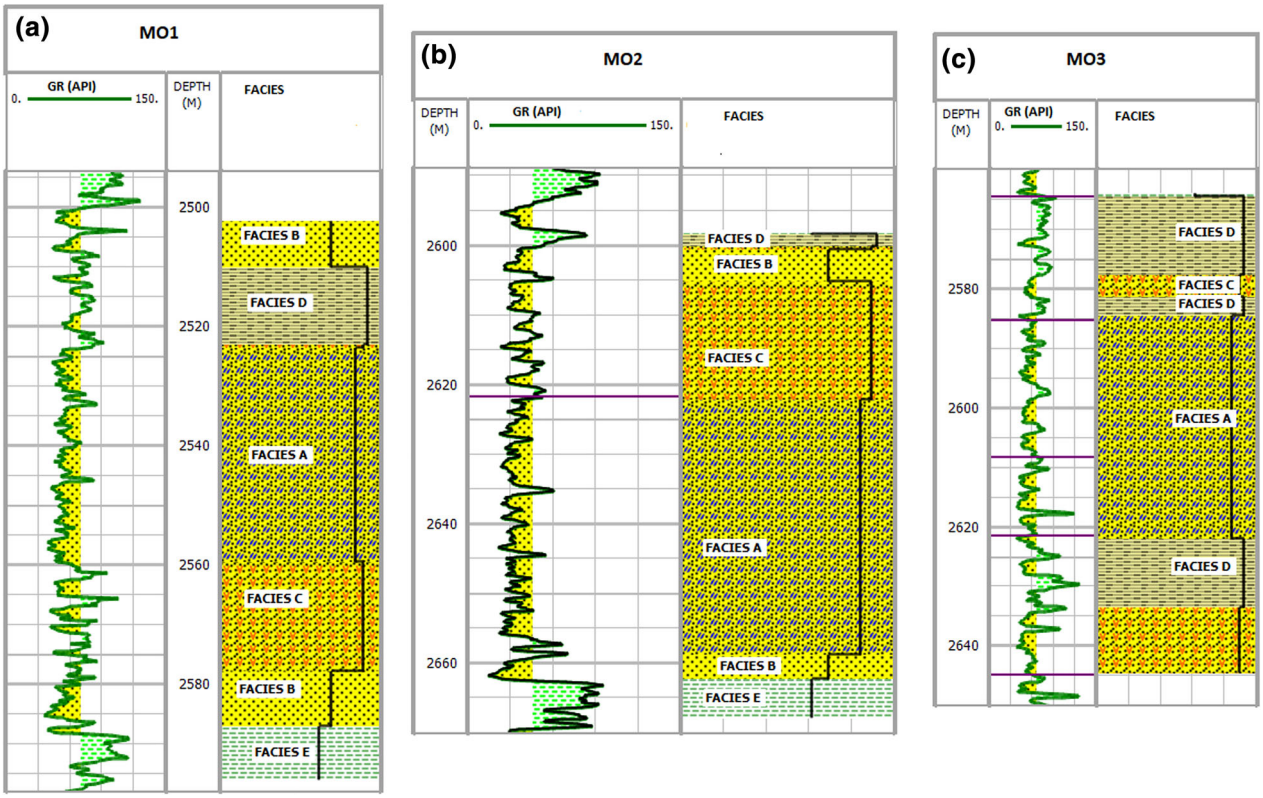

Figure 3. Facies classification showing five different facies in (**a**) well MO1 and (**b**) well MO2, and three facies in (**c**) well MO3.

Table 1. Calculated pore throat radius of rock types using the Winland r35 method, and division into five petrophysical categories. (modified after Porras et al. 1999; Opuwari et al. 2019)

Well average	Pore Throat radius (μm)	Rock type	PRT	Porosity (%)	Permeability (mD)	Regression equation	R^2
	> 10.0	Mega porous	1	13.7–20.0	93.0–956.0	$K = 5.96 \times (\text{Porosity})^{0.51}$	0.57
	2.0–10.0	Macro porous	2	12.10–17.5	9.0–93.0	$K = 8.91 \times (\text{Porosity})^{0.88}$	0.65
	0.5–2.0	Mesoporous	3	7.0–16.2	0.8–8.0	$K = 6.16 \times (\text{Porosity})^{0.72}$	0.52
	0.1–0.5	Micro porous	4	3.0–13.0	0.05–0.8	$K = 9.24 \times (\text{Porosity})^{0.23}$	0.39
	< 0.1	Nanoporous	5	< 7.0	< 0.05	Not enough data	N/A
MO1							
Minimum	0.13	Microporous	4	2.10	0.02		
Mean	5.55	Macroporous	2	13.70	13.50		
Maximum	24.41	Megaporous	1	20.10	956.00		
MO2							
Minimum	0.09	Nanoporous	5	3.30	0.02		
Mean	3.84	Macroporous	2	13.50	10.92		
Maximum	16.15	Megaporous	1	17.70	279.00		
MO3							
Minimum	0.01	Nanoporous	5	3.70	0.03		
Mean	2.86	Macroporous	2	13.40	6.05		
Maximum	16.24	Megaporous	1	18.50	459.00		
All							
Mean	4.19	Macroporous	2	13.50	8.90		

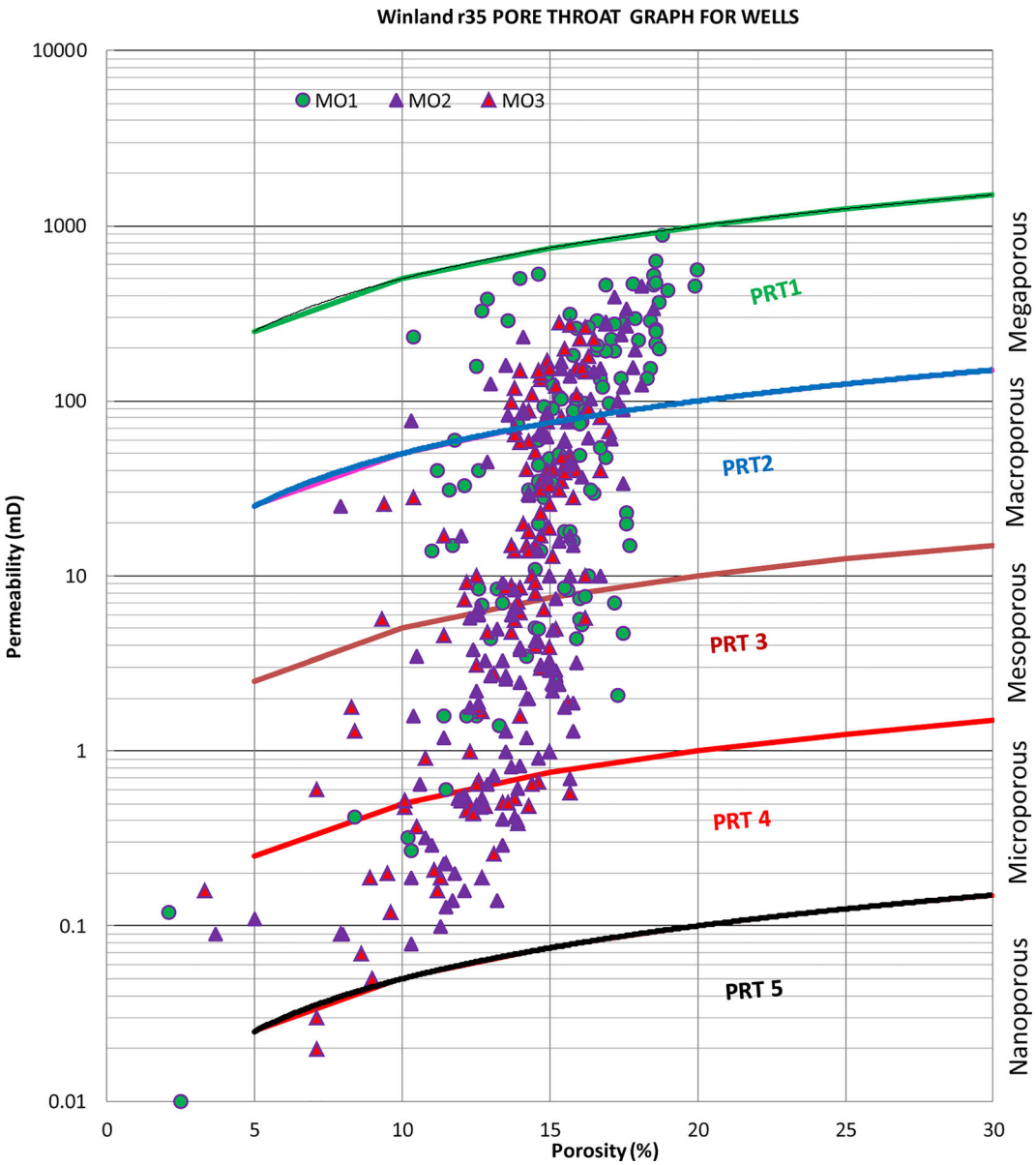

Figure 4. The Winland pore throat radius for identification of rock types.

have similar flow quality across a given range of permeability and porosity.

PRT 1 (Fig. 4) presented the most favorable fluid flow conditions that were dominated by megaporous rock types with pore throat radius greater than 10 μm, with corresponding porosity values of 13.7–20.1% and permeability values of 93–950 mD. The reservoir rock quality deteriorates from top center to bottom left, presenting PRT 5 as the one with the least reservoir rock quality. PRT 5 presented the poorest reservoir quality with pore throat radius of less than 0.1 μ, with corresponding porosity of less than 7% and permeability of 0.03 mD. The small amount of data clustered around PRT5 makes it impossible to obtain the regression equation for this rock type.

The relationship between porosity and permeability for the defined PRTs concerning the pore throat radius showed positive trends (Fig. 4), which are characterized by coefficients of determination of

R^2 = 0.57, 0.65, 0.52, and 0.39 for PRT 1 to PRT 4, respectively (Table 1). The lowest coefficient of determination for PRT 4 indicated that porosity was not the only controlling agent of permeability (Moradi et al. 2017). The other factor may be the presence of fine grain matrix or the poor sorting of pores. Petrography studies are recommended to verify the other factors controlling permeability. The permeability of a given rock is affected by many geological and petrophysical factors including lithofacies rock type, a HFU, effective porosity, and pore throat size distribution. For pore throat size, the higher the pore throat is, the better the connectivity is, the better the storage and flow capacities properties are, i.e., the better the reservoir rock type (RRT) and HFU are (El Sharawy and Nabawy 2016; Nabawy and Barakat 2017; Nabawy et al. 2018).

The individual well-to-well evaluation of calculated pore throat radius showed that well MO1 presented the best reservoir quality. This well has average pore throat radius of 5.5 μ with mean porosity of 13.7%, maximum value of 20.1%, average permeability value of 13.5 mD, and maximum value of 956 mD. The nanoporous rock type PRT5 was conspicuously absent in this well.

Well MO2 showed good reservoir quality with a mean pore throat radius of 3.84 μ, which makes it a macroporous rock type. The mean porosity of this well was 13.5%, and its average permeability was 10.92 mD. The nanoporous rock type was observed in this well. However, for well MO3, the mean pore throat radius was 2.86 μ, with porosity value of 13.4% and average permeability of 6.0 mD.

The overall assessment shows that the best reservoir quality was found clustering in the center top that comprised all the wells. Intermediate reservoir quality rocks (PRT 2 and PRT 3) were found in the middle part made up of all the wells. Based on the results from the Winland r35 method, we thus proposed a porosity of 7% and a permeability of 0.1 mD as the cutoff for the gas field.

HFU Determination Using the FZI

The computation of HFUs, using the FZI and the potential reservoir index (PRI) for ranking, was achieved by the application of Eqs. 2 to 5. The computations of FZI and PRI for the studied wells using the modified classification criteria of Nabawy and Al-Azazi (2015) resulted in four distinct HFUs (Table 2). The log–log plot of RQI vs. NPI with the application of HFU criteria listed in Table 2 identified four distinguishable HUs in terms of FZI (Fig. 5). The RQI and FZI were somewhat related to the effective pore radius that was responsible for fluid flow and reservoir quality. The FZI discriminating lines were calculated based on the classification introduced by Nabawy and Al-Azazi (2015). The best values of RQI and FZI correspond to well MO1 (average 0.58 and 3.19 μ, respectively, which refer to good reservoir quality rank (Table 2). Conversely, well MO3 had the least reservoir quality (average RQI of 0.32 μ and FZI of 1.9 μ) indicating poor reservoir quality rank represented by RPI rank of 1.1 (Table 2).

HFU-2, with FZI between 2.5 and 5 μ, was ranked as good rock type. HFU-3 had FZI in the range of 1.0 to 2.5 μ, and it was ranked as fair rock type. Rock types with FZI of less than 1 μ are ranked poor and impervious rock types and fall into the HFU-4 group. The RQI vs. NPI plots for the defined PRTs showed positive trends (Fig. 5), with coefficients of determination of 0.60, 0.58, 0.68, and 0.52 for HFU-1 to HFU-4, respectively (Table 2). These HFU identification criteria were adopted on an individual well basis to understand the spread of HFU and to identify the best HFU.

Well MO1 presented the best reservoir quality with average FZI of 3.19 μ, which was ranked as good, whereas well MO2 had average FZI of 2.3 μ, which was also ranked as good. In comparison, well MO3 showed average FZI of 1.90 μ and it was ranked as fair. The overall assessment showed that FZI of all well ranged from 0.03 to 13.45 μ with average of 2.52 μ and average RPI of 1.39, thereby ranking the studied wells as fair. The identified HFUs were present in all the wells, and HFU-4 was ranked as poor or impervious rock type.

SMLP and FUE

The SMLP was performed to know the variability of permeability in a reservoir interval and to reveal the portion of the reservoir that contributes to the flow (Gunter et al. 1997). The Lorenz coefficient ranges from zero to one. An interval of uniform permeable reservoir has a Lorenz coefficient of zero (Pranter et al. 2004). The point of inflexions on the curve represents speed, baffle, or barrier zones. The preliminary flow and storage units were interpreted on an individual well basis by selecting significant changes in slope or inflexion points (Fig. 6a–c).

Table 2. Subdivision of FZI groups into three HFUs for the studied wells, using the modified classification criteria. (Nabawy and Al-Azazi 2015; Nabawy et al. 2018)

Well statistics	NPI (v/v)	RQI (μm)	FZI (μm)	RPI (ranking)	HFU	Regression equation	R^2
	0.10–0.25	0.5–2.25	> 5.00	> 4.0 Very good	1	RQI = 52.4 $(NPI)^{2.8}$	0.60
	0.08–0.21	0.30–1.00	2.50–5.0	3–3.5 Good	2	RQI = 0.75 $(NPI)^{0.87}$	0.58
	0.026–0.21	0.05–0.50	1.00–2.5	2.0–2.9 Fair	3	RQI = 18.52 $(NPI)^{2.4}$	0.68
	0.022–0.21	0.02–0.20	< 1.00	< 1.00 Poor	4	RQI = 0.53 $(NPI)^{0.42}$	0.52
MO1							
Minimum	0.02	0.02	0.17	0.10	4		
Mean	0.16	0.58	3.19	1.89	2		
Maximum	0.25	2.25	13.45	7.62	1		
MO2							
Minimum	0.06	0.01	0.13	0.07	4		
Mean	0.16	0.42	2.30	1.45	2		
Maximum	0.20	1.60	8.07	4.83	1		
MO3							
Minimum	0.04	0.003	0.03	0.02	4		
Mean	0.16	0.32	1.90	1.12	3		
Maximum	0.23	1.58	7.76	4.52	1		
All							
Minimum	0.02	0.003	0.03	0.02	4		
Mean	0.16	0.41	2.52	1.39	3		
Maximum	0.25	2.25	13.45	7.62	1		

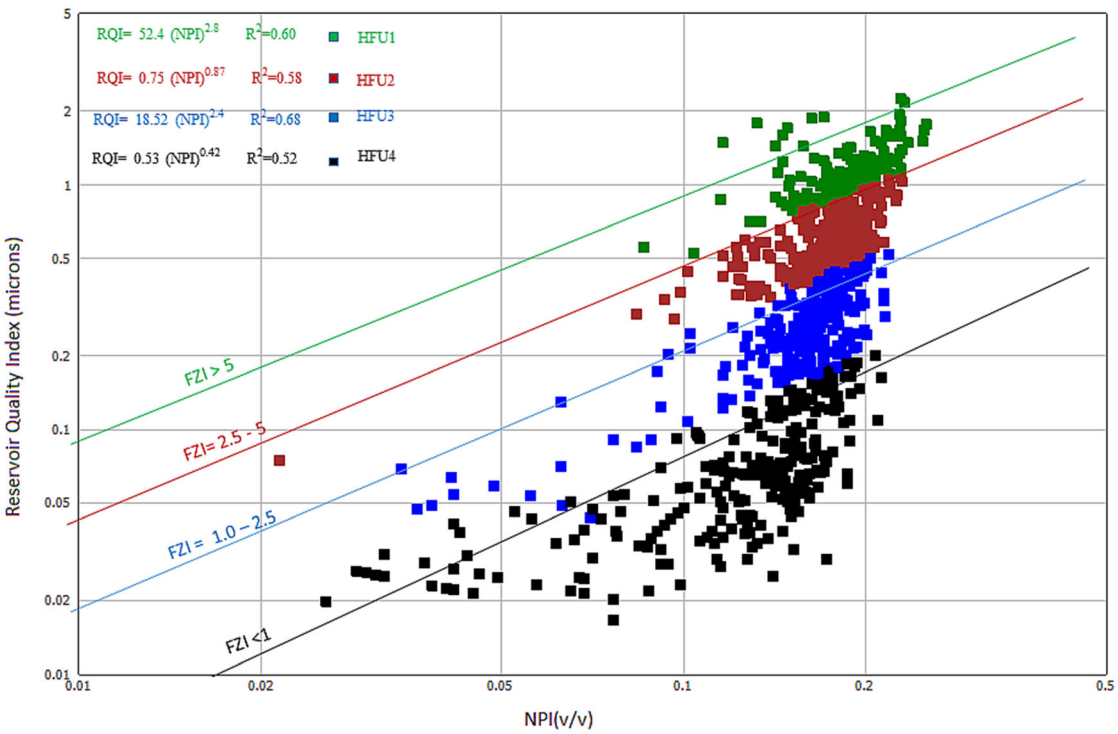

Figure 5. Log–log plot of RQI vs. NPI for FZI, showing four different rock classifications.

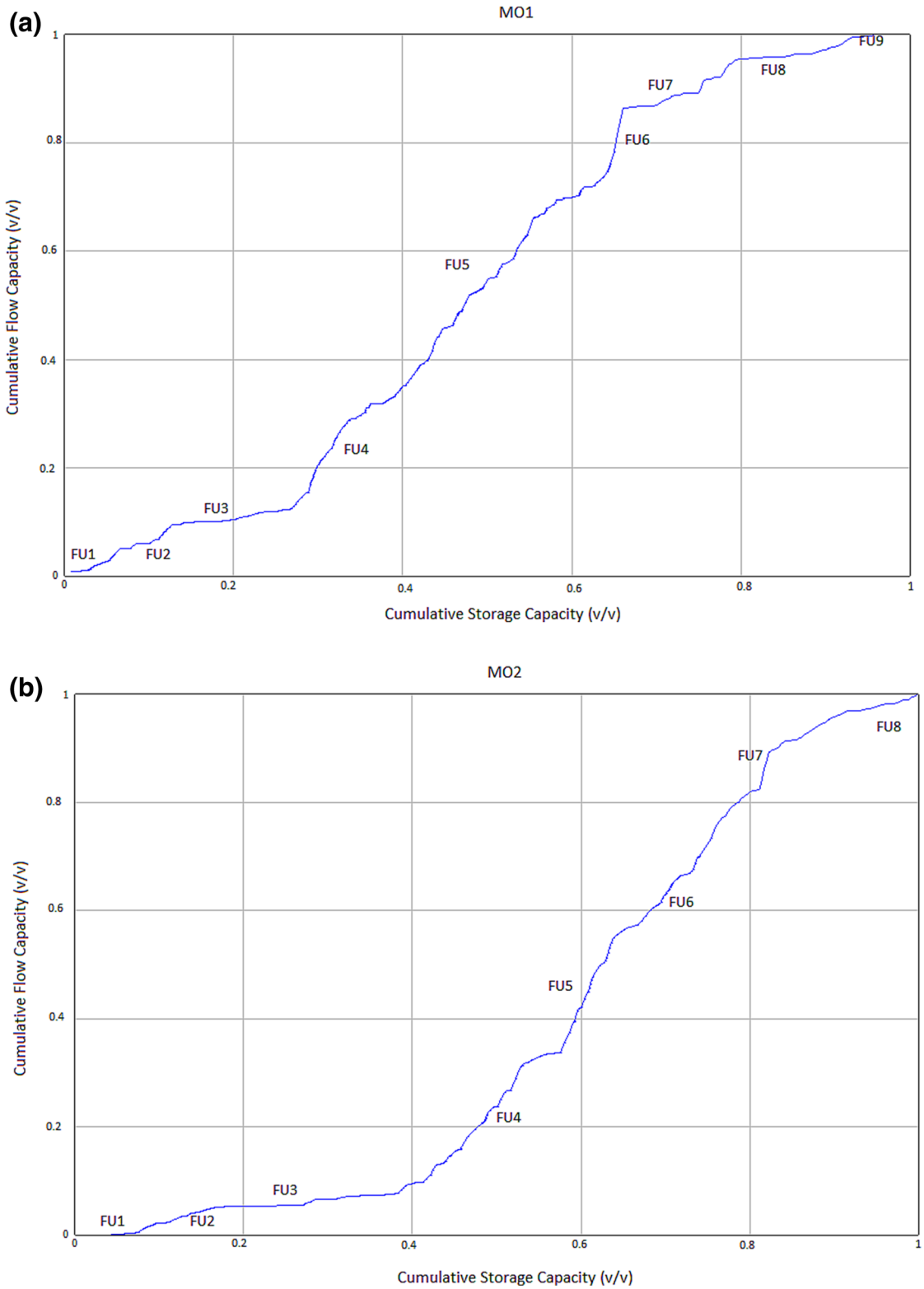

Figure 6. Cross-plots of cumulative storage capacity vs. cumulative flow capacity for wells (**a**) MO1, (**b**) MO2, and (**c**) MO3, which show different FUs determined from SMLP.

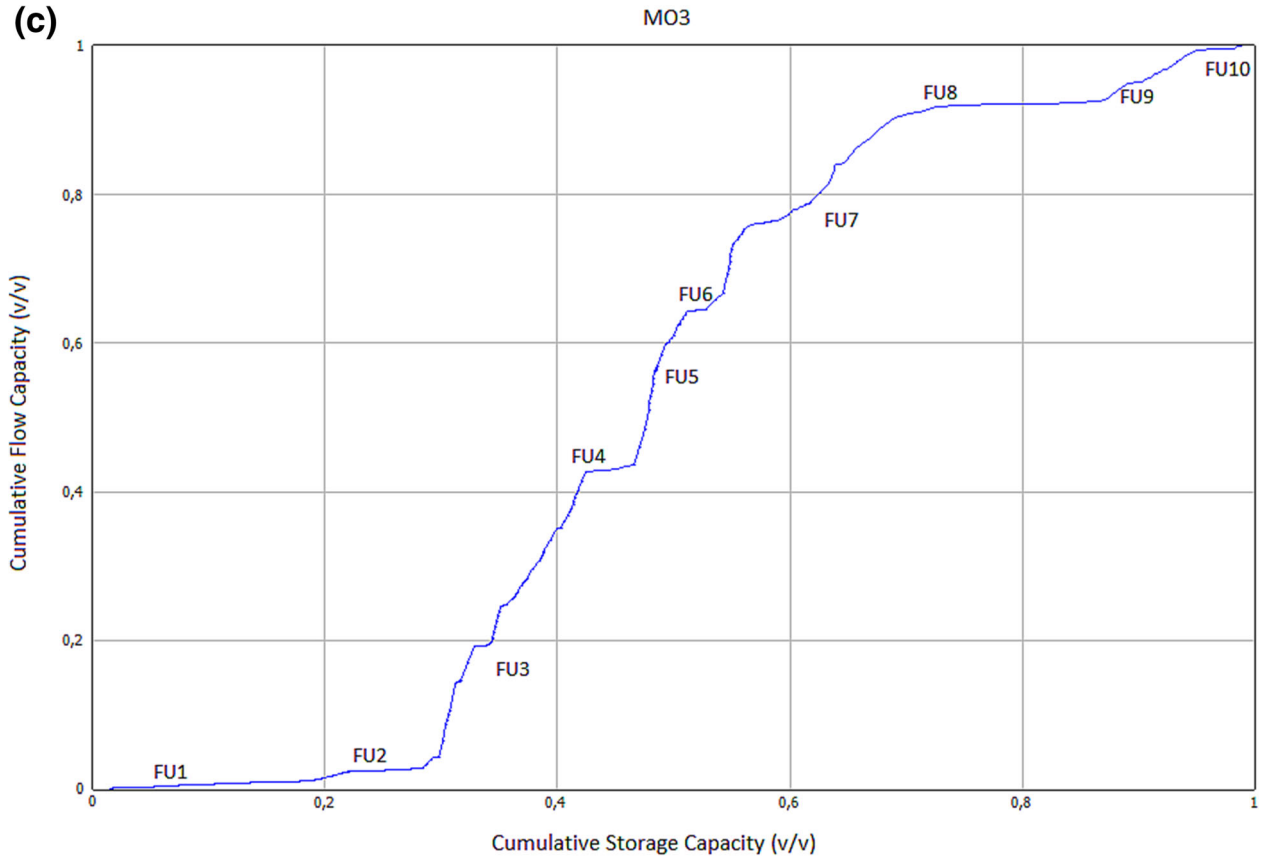

Figure 6. continued.

The results of the SMLP for well MO1 (Fig. 6a) presented nine FUs from bottom to top. FUs 4, 5, and 6 all had the same FUE, and they collectively contributed to 73% of the flow capacity and to 40% of the storage capacity. FUs 2, 7, and 8 were the slow ones and were regarded as the baffle unit, as they collectively accounted for 27% of the flow capacity and 42% of the storage capacity. FUs 1, 3, and 9 were seals, and they did not contribute to the flow, but they had 18% of the storage capacity. Well MO2 (Fig. 6b) presented eight FUs, of which FUs 4, 5, and 6 all had the same flow efficiency regime and they contributed collectively to 68% of the flow capacity and to 41% of the storage capacity. FUs 2, 3, and 7 were the slow efficiency units (baffle), and they contributed collectively to 32% of the flow capacity and to 58% of the storage capacity. FUs 1 and 8 had no flow capacity but had a storage capacity of 2%. Ten FUs are for well MO3 (Fig. 6c). FUs 3, 5, and 7 were the efficient ones and accounted for 70% of the flow capacity and for 46% of the storage capacity. The slow efficiency zones were FUs 2, 8, and 9 and they contributed collectively to 15% of the flow capacity and to 54% of the storage capacity, while FUs 1, 4, and 9 were the zero FUs, but they accounted for 18% of the storage capacity.

To understand the reservoir zone performance of a well, the differences in storage and flow capacity play a prominent role (Bhattacharya et al. 2008). The FUE was constructed from the ratio of cumulative flow capacity to cumulative storage capacity. The FUE related the differences in the percentage flow to storage capacity, which enabled the delineation of a high-efficiency zone from that of a low efficiency zone of the individual wells. The reservoir intervals were subdivided into a FUE character as a function of depth for each well (Fig. 7a–c). The FU of high efficiency shows FUE values greater than 0.8 (Table 3) and a permeability of 100 mD. The fluid in the reservoir was considered to move fast in a high FUE zone (Fig. 7a) because of the presence of good quality reservoir rock. The moderate FUE zones (Fig. 7b, c) were fine- to medium-grained sandstone with minor shales, moderately cemented with per-

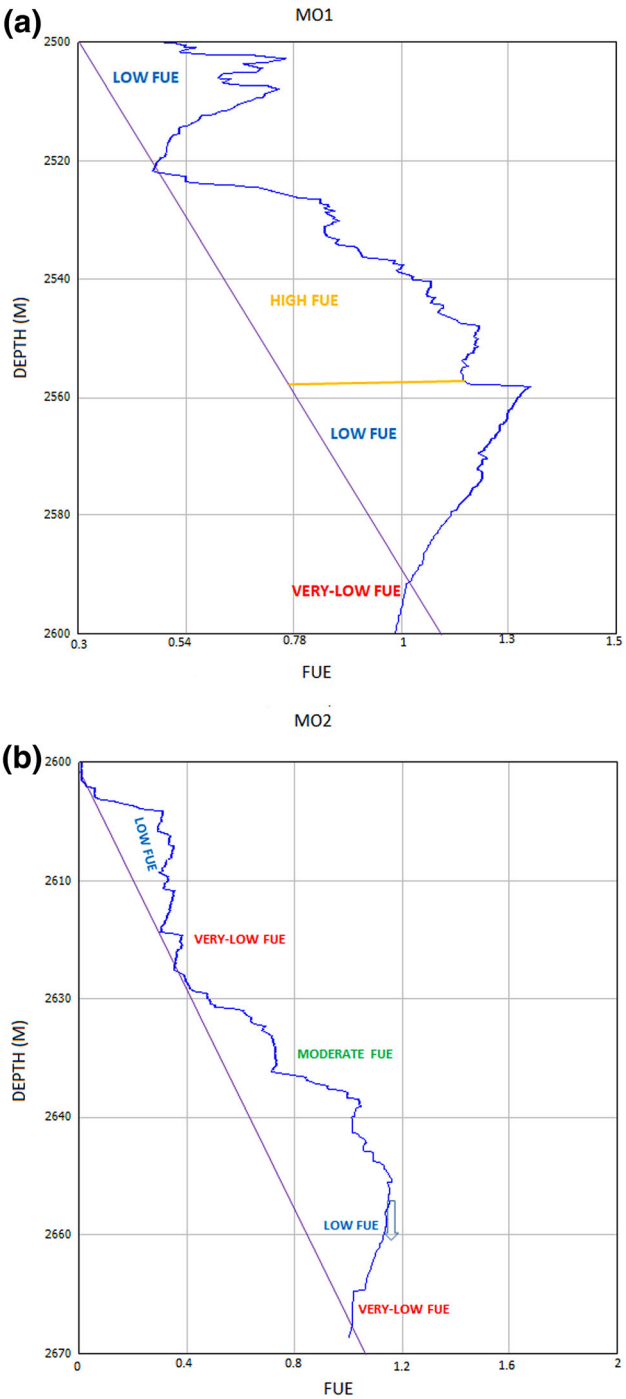

Figure 7. Plots of FUE vs. depth for wells (**a**) MO1, (**b**) MO2, and (**c**) MO3. The segregation of different flow zones are indicated at their appropriate positions.

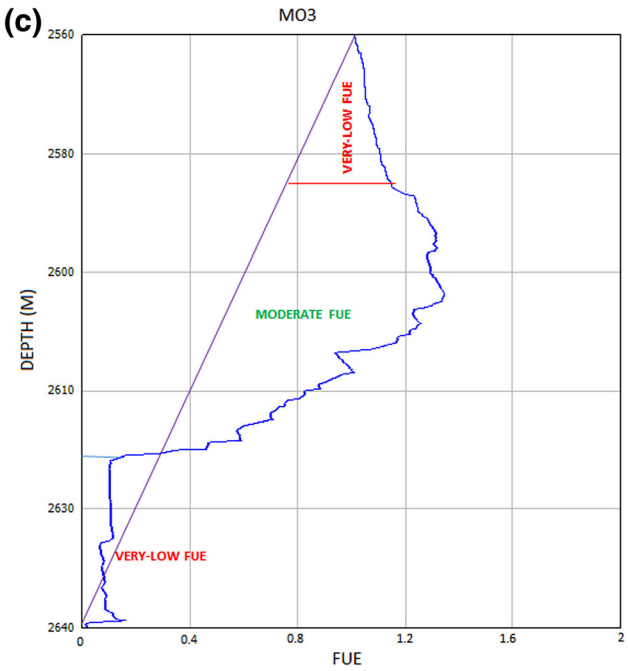

Figure 7. continued.

Table 3. Developed zonation scheme used for the identification of high speed and low speed flow zones

Well	Top depth (m)	Bottom depth (m)	Thickness (m)	HU	Porosity %	Permeability mD	r35 (μm)	FZI (μm)	Zone/unit	Facies	Storage (%)	Flow (%)	FUE
					15–20	50–250	> 10	> 5	High		> 10	> 50	≥ 0.8–1.6
					10–15	10–50	5–10	3–5	Moderate		> 10	20–50	0.4–0.8
					5–10	1–10	2–5	2–3	Low		≤ 10≥	10–20	0.2–0.4
					< 5	≥ 1	1–2	1–2	Very low		< 10	< 5	≤ 0.2
					< 5	< 1	< 1	< 1	Tight				
MO1	2504.1	2522.2	18.1	1	15.6	25.3	4.2	2.9	Low	B/D	18.2	10.0	0.3
	2522.2	2558.0	35.8	2	15.1	99.7	10.0	5.1	High	A	40.0	73.0	0.8
	2558.0	2587.0	29.0	3	13.6	10.3	3.5	2.2	Low	B/C	41.8	17.0	0.2
	2587.0	2596.0	9.0	4	5.4	0.04	0.2	0.6	Tight	E	0	0	
MO2	2600.1	2609.5	9.4	1	13.7	9.3	2.3	1.6	Low	B	18.0	10.0	0.2
	2609.5	2620.7	11.2	2	13.0	2.3	1.7	1.2	Very low	C	16.0	4.0	0.1
	2620.7	2649.3	28.6	3	13.8	39.4	5.9	3.6	Moderate	A	41.5	68.0	0.6
	2649.3	2662.1	12.8	4	13.5	17.5	3.4	2.3	Low	B	23.0	17.0	0.2
	2662.1	2668.2	6.1	5	9.7	0.3	0.6	0.6	Tight	E	1.5	1.0	Nil
MO3	2564.4	2585.2	20.8	1	13.6	1.6	0.9	0.8	Very low	D/C	20.0	9.5	0.1
	2585.2	2621.3	36.1	2	14.1	26.8	5.4	3.3	Moderate	A	46.0	70.0	0.6
	2621.3	2644.7	23.4	3	12.1	2.3	1.6	1.0	Very low	D/C	34.0	8.5	0.1

meability (27–40 mD) and FUE of 0.6. The fluid in the reservoir will move slower in this zone than in the high zone. Conversely, gas in the reservoir will move slow and very slow in the low FUE and very low FUE zones, respectively, which indicate FUE values of less than 0.4 and permeability of less than 27 mD (Fig. 7a–c). Our FUE plot can be compared directly to flowmeter logs.

Integration of the FU Methods for the Development of a Zonation Scheme

The integration of facies using two petrophysical methods of rock type classification, namely HU (Winland r35 and FZI) and FU (SMLP and FUE) method, was presented alongside each other. Results indicate that the HU method can be adopted to identify vertical flow zones because it presents better results for vertical zonation. The FU method differs in some cases from the HU method in that they are bounded by a significant change in permeability, whereas the HU is bounded by barriers to vertical flow. Therefore, the FUE was adopted to identify FU efficiencies. The concepts of a rough field guide to porosities in reservoirs (Levorsen and Berry 1967) and a permeability classification scale (Tiab and Donaldson 2015) were modified here into a scheme for reservoir zonation. In this regard, 12 reservoir zones were distinguished as high, moderate, low, very low, and tight zones (Table 3).

Figures 8, 9, and 10 illustrate the comparison of the results from the HU and the FU methods. There is relatively good correspondence between the results of these two methods. Well MO1 had a reservoir thickness of 90.0 m and comprised eight zones. However, in the distribution of zone thicknesses, the results of HU and FU methods were significantly different in zones (Fig. 8). Zone 1 was observed at the upper part of the reservoir at depths of 2504.1–2522.2 m (18.1 m thick) and was considered as the low zone. This zone comprised facies B and D and had an average porosity of 16% and permeability of 25 mD. The reservoir quality of the zone was that of a macroporous rock composed of good reservoir quality HFU-2 rock type. Additionally, this zone corresponded to FU2 and FU3 with storage capacity of 18% and flow capacity of 10%. The Winland r35 method grouped this zone as megaporous rock (good reservoir quality), while FZI classifies this zone as HFU-3 (fair reservoir quality) rock. However, the SMLP method classified this as a barrier to flow (FU3), which agrees with the FZI method. The FZI method agrees with the SMLP method. Therefore, the zone was interpreted as barrier to flow from a high flow zone to below this zone.

The high flow zone, located at depths of 2522.2–2558.0 m (35.8 m thick), was bounded vertically at the bottom by a low zone. This zone had streaks of high GR values because of the minor shales intercalation, and well-cemented fine- to medium-grain sandstone associated with facies A. An average porosity and average permeability of 15% and 100 mD, respectively, were recorded in this zone (Table 3). This zone comprised high quality PRT1 and HFU-1 with storage capacity of 40%, flow capacity of 73%, and FUE of 0.8. Below this high zone was a low zone located at depths of 2558.0–2587.0 m, composed of facies C and B. An average porosity of 14% and average permeability of 10 mD were dominated by mesoporous and HFU-3 rock types grouped as fair reservoir rock quality. Facies C at the upper part of this zone provided sand–sand contacts allowing the transfer of flow between the low and high zones. Our interpretation is supported by Larue and Legarre 2004). This zone was significant because it demarcated the high zone from the very low zone. The rock quality depreciated from this low zone down to the base of the reservoir (tight zone), which was due to the smaller pore throat radius and the decline in permeability.

Well MO2 had a reservoir thickness of 68.1 m and included five zones of low, very low, moderate, low, and tight (Fig. 9). Two low flow zones were located at depths of 2600.1–2609.5 m at the upper part of the reservoir and at depths of 2649.3–2662.1 m at the lower part. Both zones were composed of facies B but differed in the Winland r35 grouping, while FZI classified both as medium reservoir quality rock (HFU-3). The FU method classified both zones as baffle with low flow efficiency, which agrees with the FZI method. The low flow zones were bounded vertically at the bottom by very low and tight zones at depths of 2609.5–2620.7 m and 2622.1–2688.2 m, which were composed of facies C and E, respectively. The tight flow zone was the lowest reservoir quality, having the lowest flow efficiency.

The best reservoir quality rock for well MO2 was in the middle part of the reservoir at depths of 2620.7–2640.6 m and was delineated as a moderate zone (Fig. 9). This zone had an average porosity of 14% and average permeability of 39 mD, which comprised facies A, megaporous rock type, and

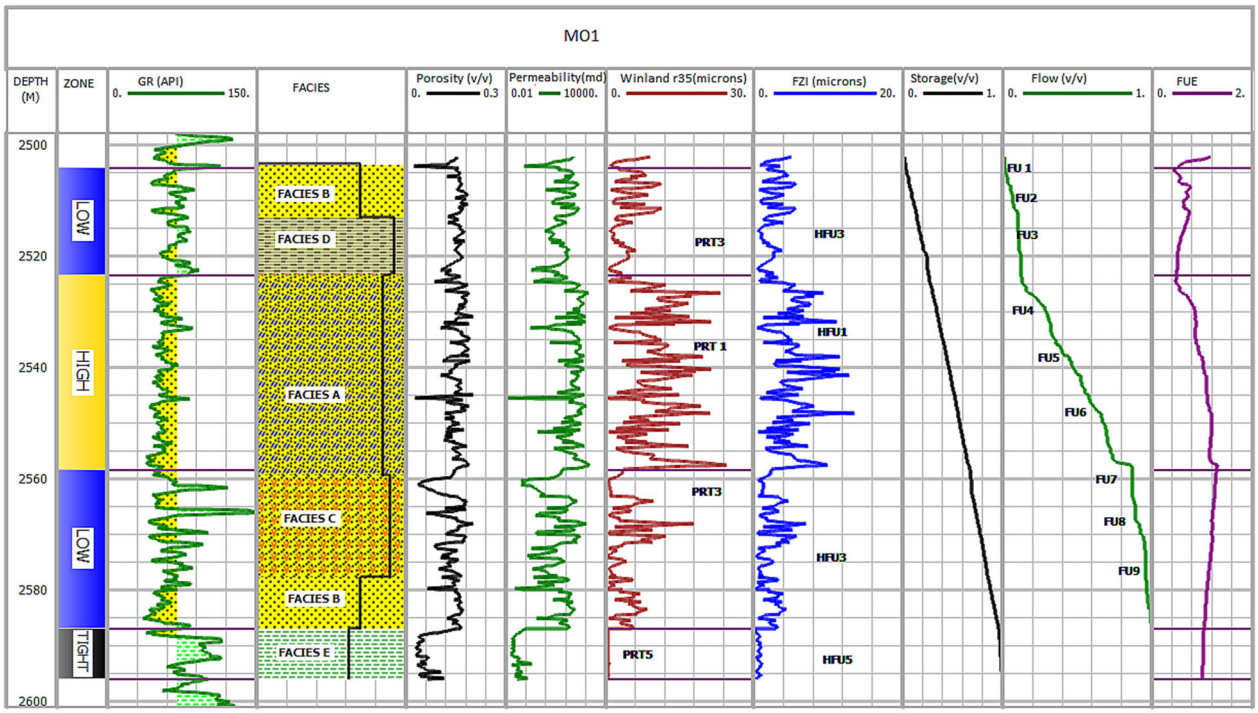

Figure 8. Integrated results for well MO1 showing facies in track 4, Winland pore throat radius in track 7, HFU determination using FZIs in track 8, and SMLP of cumulative storage and flow capacities in tracks 9 and 10, and FUE in track 11.

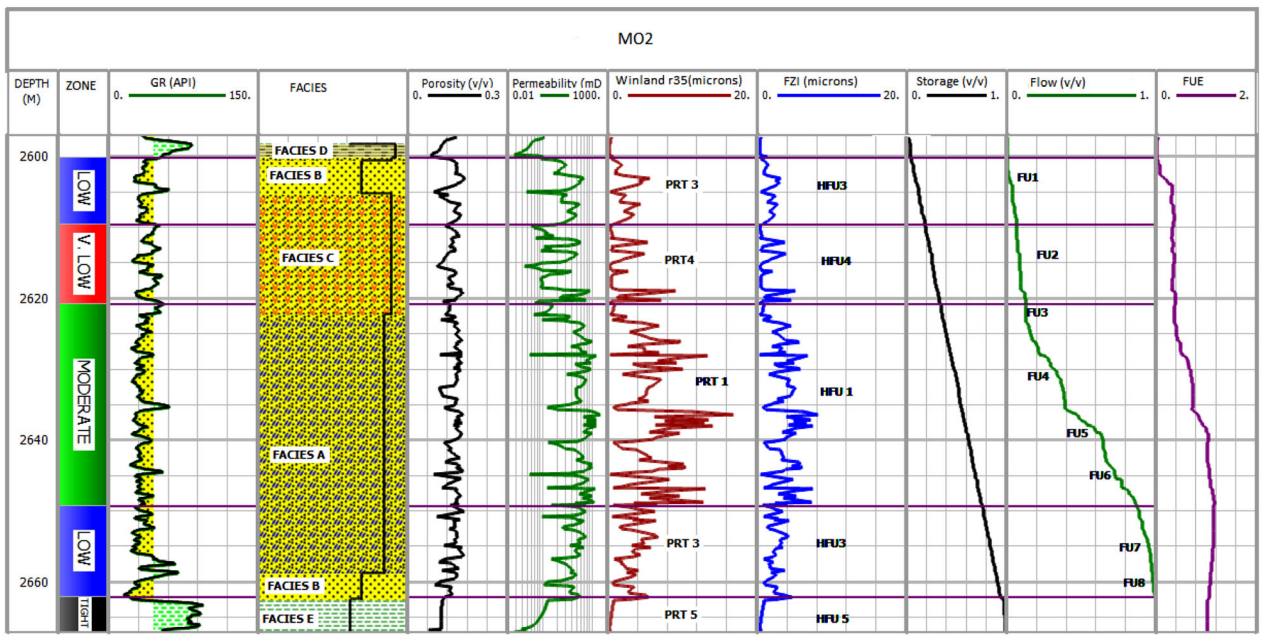

Figure 9. Integrated results for well MO2 showing facies in track 4, Winland pore throat radius in track 7, HFU determination using FZIs in track 8, and SMLP of cumulative storage and flow capacities in tracks 9 and 10, and FUE in track 11.

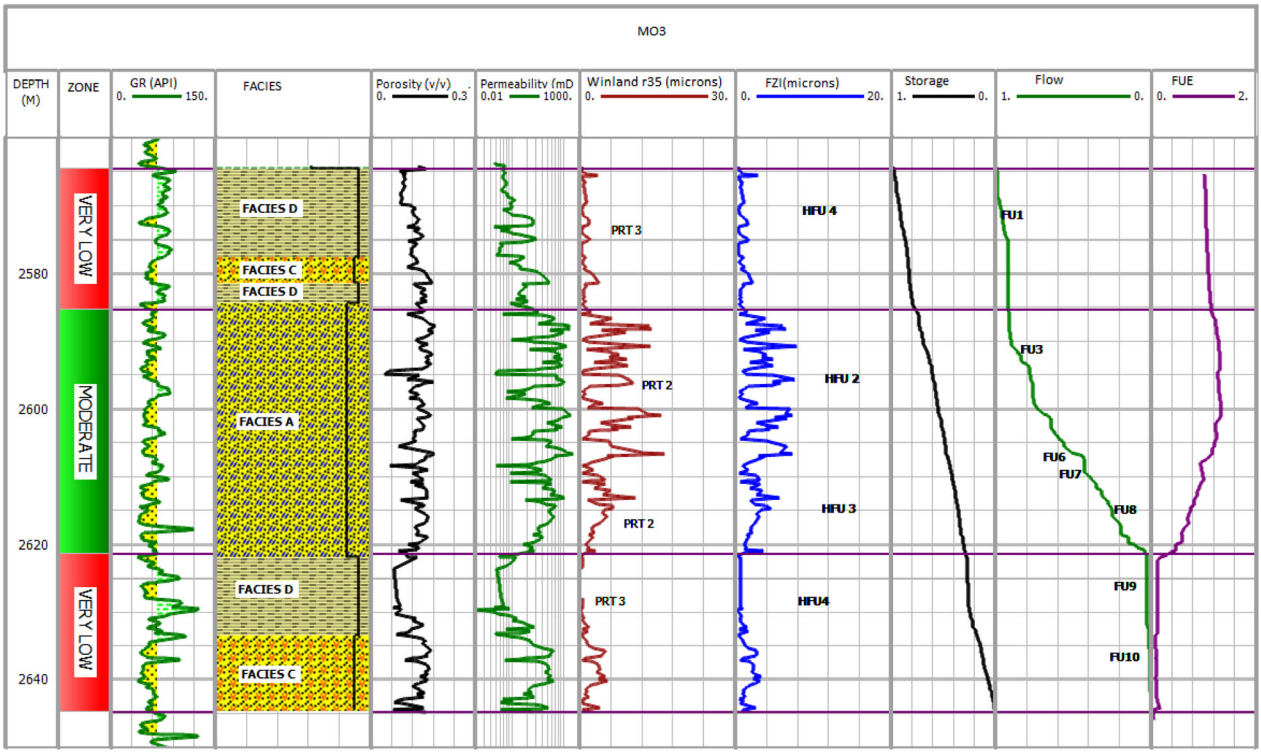

Figure 10. Integrated results for well MO3 showing facies in track 4, Winland pore throat radius in track 7, HFU determination using FZIs in track 8, and SMLP of cumulative storage and flow capacities in tracks 9 and 10, and FUE in track 11.

HU2. The moderate zone contributed 80% to the flow and had a 42% storage capacity. The low flow zone bounded this zone at the base of the zone (2649.3–2662.1 m) of facies A and C, provided sand–sand contacts allowing the transfer of flow between the moderate and the low zone.

Well MO3 had a reservoir thickness of 80.3 m and was composed of three zones of very low and moderate (Fig. 10) flow zones. Two very low flow zones were located at the top and at the bottom of the reservoir at depths of 2564.4–2585.2 m and 2621.3–2644.7 m, respectively. The average porosity and average permeability of the upper very low zone were 13.6% and 1.6 mD, respectively. The very low zone at the base of the reservoir had average porosity and average permeability of 12.1% and 2.3 mD, respectively. The zone was composed of facies C and D and was designated as the lowest reservoir quality rock, also having the lowest flow efficiency. The moderate flow zone sandwiched between the very low zones was the best quality rock composed of facies A. The average porosity and average permeability of the moderate zone were 14% and 27 mD, respectively, and it had a storage and a flow capacity of 46% and 70%, respectively.

An observed pattern in this study was that the facies did not always coincide with the flow zones, and that the FZI method was more reliable for the determination of a HU. A general decline in porosity and permeability with depth reflects a decrease in reservoir quality, a theory which is supported by many that decreasing porosity and increasing cementation with depth in the rock hosting hydrocarbon column (Gluyas et al. 1993). Comparison of the results shows that integration of the HU and the FU methods provided better and reliable output for flow zone identification from core data. The FUE played a significant role in the segregation of the flow zones.

The three generalizations deduced from the relationship between FUs and facies are as follows. Firstly, the reservoir FUs of best quality are located in the middle to the upper parts of the reservoirs. Secondly, high quality flow zones are associated with

facies A; conversely, the reservoir rocks of lowest quality are composed of facies E, while facies C and B are reservoir rock types of intermediate quality. Thirdly, in this study, it was revealed that smaller pores are the lowest reservoir quality rock, while larger pores are the best quality reservoir rock. Therefore, for robust identification of flow in a reservoir, we first need to determine various HUs, each representing a unique pore throat characteristic, and then predict flow efficiency.

CONCLUSION

Flow zone identification from core data in the Western Bredasdorp Basin Offshore in South Africa was performed by two independent methods, namely HU (Winland r35 and FZI) and FU (SMLP and FUE). Lithofacies were identified firstly by using sedimentology report and gamma-ray log responses, and secondly by using the HU and FU methods. The results of the two methods showed reasonable correlation. By integration of the rock type results from these methods, a reservoir zonation scheme was developed for the sandstone reservoirs of the gas field. For a zone to be ranked as high efficiency, it must have an optimum average pore throat radius of $> 10.0\ \mu$, FZI of > 5.0, and FUE of > 8. An average flow efficiency of 0.8 separates a high-efficiency zone from other zones.

Twelve flow zones identified with well MO1 as having high flow efficiency were the best reservoir quality rock associated with facies A. The tight zones were the lowest reservoir quality associated with facies E. Facies C, which is fine to very fine-grained sandstone, provides sand–sand contacts that allow transfer of flow between moderate and low zones. The reservoir flow zone of best quality was located in the middle to upper parts of the reservoirs. In this study, smaller pores were the lowest reservoir quality rock, while larger pore was the best quality reservoir rock. Therefore, for a robust identification of flow in a reservoir, we first need to determine various HUs, each representing a unique pore throat characteristic, and then predict flow efficiency. This plays a significant role in the identification of flow zones.

The results from this study will help reduce the necessity to upscale a static geological model for reservoir simulation in the western Bredasdorp Basin in South Africa. The future work to be done from this work is to perform mineralogical analyses of rocks from the identified zones in order to understand the effects of mineralogy on petrophysical properties. Additionally, production test analyses are recommended to verify if the flow zones are in the same pressure regime or if they are isolated vertically/laterally and the type of fluid that saturates each zone.

ACKNOWLEDGMENTS

The authors would like to thank the Petroleum Agency of South Africa (PASA) for providing the data used in this work. The Synergy Company is also acknowledged for the provision of an IP software package. The authors would like to thank the anonymous reviewers for their significant comments that helped us reconstruct and improve the manuscript. Special thanks to the Editor for providing valuable suggestions to the revised manuscript.

REFERENCES

Abuseda, H., Kassab, M. A., LaLa, A. M., & El Sayed, N. A. (2015). Integrated petrographical and petrophysical studies of some Eocene carbonate rocks, Southwest Sinai, Egypt. *Egyptian Journal of Petroleum, 24*(2), 213–230.

Acho, C. B. (2015). *Assessing hydrocarbon potential in cretaceous sediments in the Western Bredasdorp Sub-basin in the Outeniqua Basin South Africa*. The University of the Western Cape, South Africa student thesis. Retrieved March 24, 2020, from http://etd.uwc.ac.za/handle/11394/4807.

Aguilera, R. (2014). Flow units: From conventional to tight-gas to shale-gas to tight-oil to shale-oil reservoirs. *SPE Reservoir Evaluation & Engineering, 17*(02), 190–208.

Amaefule, J. O., Altunbay, M., Tiab, D., Kersey, D. G., & Keelan, D. K. (1993). Enhanced reservoir description: Using core and log data to identify hydraulic (flow) units and predict permeability in uncored intervals/wells. In *SPE annual technical conference and exhibition*. Society of Petroleum Engineers.

Archie, G. E. (1950). Introduction to petrophysics of reservoir rocks. *AAPG Bulletin, 34*(5), 943–961.

Bhattacharya, S., Byrnes, A. P., Watney, W. L., & Doveton, J. H. (2008). Flow unit modelling and fine-scale predicted permeability validation in Atokan sandstones: Norcan East field, Kansas. *AAPG Bulletin, 92*(6), 709–732.

Boada, E., Barbato, R., Porras, J. C., & Quaglia, A. (2001). Rock typing: Key approach for maximising the use of old well log data in mature fields, Santa Rosa field, case study. In *SPE Latin American and Caribbean petroleum engineering conference*. Society of Petroleum Engineers.

Broad, D. S., Jungslager, E. H. A., McLachlan, I. R., & Roux, J. (2006). Offshore Mesozoic basins. *The Geology of South Africa. Geological Society of South Africa, Johannesburg/ Council for Geoscience, Pretoria* (pp. 553–571).

Brown, L. F., Benson, J. M., Brink, G. J., Doherty, S., Jollands, A., Jungslager, E. H. A., et al. (1996). Sequence stratigraphy in

offshore South Africa divergent basins. An atlas on exploration for cretaceous lowstand traps by SQEKOR (Pty) Ltd. *American Association of Petroleum Geologists, AAPG Studies in Geology, 41,* 184.

Carman, P. C. (1937). Fluid flow through granular beds. *Transactions Institute of Chemical Engineers, 15,* 150–166.

Cerepi, A., Barde, J.-P., & Labat, N. (2003). High-resolution characterization and integrated study of a reservoir formation: The Danian carbonate platform in the Aquitaine Basin (France). *Marine and Petroleum Geology, 20*(10), 1161–1183.

Chekani, M., & Kharrat, R. (2009). Reservoir rock typing in a carbonate reservoir-cooperation of core and log data: A case study. In *SPE/EAGE reservoir characterization & simulation conference* (pp. cp–170). European Association of Geoscientists & Engineers.

Chopra, A. K., Stein, M. H., & Ader, J. C. (1987). Development of reservoir descriptions to aid in the design of EOR projects. In *SPE California regional meeting*. Society of Petroleum Engineers.

Corbett, P. W. M., Ellabad, Y., & Mohammed, K. (2001). The recognition, modelling and validation of hydraulic units in the reservoir rock. In *3rd institute of mathematics and its applications conference on modelling permeable rocks* (pp. 27–29).

Corbett, P. W. M., & Potter, D. K. (2004). Petrotyping: A base map and atlas for navigating through permeability and porosity data for reservoir comparison and permeability prediction. In *Paper SCA2004-30 presented at the international symposium of the society of core analysts* (Vol. 5).

Das, B., & Chatterjee, R. (2018). Well log data analysis for lithology and fluid identification in Krishna-Godavari Basin, India. *Arabian Journal of Geosciences, 11*(10), 231.

Davies, C. P. (1997). Unusual biomarker maturation ratio changes through the oil window, a consequence of varied thermal history. *Organic Geochemistry, 27*(7–8), 537–560.

Ebanks Jr, W. J. (1987). Flow unit concept-integrated approach to reservoir description for engineering projects. *AAPG (American Association of Petroleum Geologists) Bulletin; (United States)*, *71*(CONF-870606-).

Eichkitz, C. G., Schreilechner, M. G., Amtmann, J., & Schmid, C. (2009). Shallow seismic reflection study of the Gschliefgraben landslide deposition area-interpretation and three dimensional modeling. *Austrian Journal of Earth Sciences, 102*(2), 52–60.

El Sharawy, M. S., & Nabawy, B. S. (2016). Geological and petrophysical characterisation of the lower Senonian Matulla formation in Southern and Central Gulf of Suez, Egypt. *Arabian Journal for Science and Engineering, 41*(1), 281–300. https://doi.org/10.1007/s13369-015-1806-7.

El Sharawy, M. S., & Nabawy, B. S. (2019). Integration of electrofacies and hydraulic flow units to delineate reservoir quality in uncored reservoirs: A case study, Nubia Sandstone Reservoir, Gulf of Suez, Egypt. *Natural Resources Research, 28*(4), 1587–1608.

Ellabad, Y., Corbett, P. W. M., & Straub, R. (2001). *Hydraulic units approach conditioned by well testing for better permeability modelling in a North Africa oil field*. Paper SCA (Vol. 50).

Elliott, T. (1997). Brown, LF, Jr., Benson, JM, Brink, GJ, Doherty, S., Jollands, A., Jungslager, EHA, Keenan, JHG, Muntingh, A. & Van Wyk, NJS 1995. Sequence Stratigraphy in Offshore South African Divergent Basins. An Atlas on Exploration for Cretaceous Lowstand Traps by Soekor (Pty) Ltd. AAPG Studies in Geology Series no. 41. Tulsa: American Association of Petroleum Geologists. P ISBN 0 89181 049 8. *Geological Magazine, 134*(1), 121–142.

Gluyas, J. G., Robinson, A. G., Emery, D., Grant, S. M., & Oxtoby, N. H. (1993). The link between petroleum emplacement and sandstone cementation. In *Geological society, London, petroleum geology conference series* (Vol. 4, pp. 1395–1402). Geological Society of London.

Gomes, J. S., Ribeiro, M. T., Strohmenger, C. J., Naghban, S., & Kalam, M. Z. (2008). Carbonate reservoir rock typing-the link between geology and SCAL. In *Abu Dhabi international petroleum exhibition and conference*. Society of Petroleum Engineers.

Grier, S. P., & Marschall, D. M. (1992). Reservoir quality: Part 6. Geological methods. *American Association of Petroleum Geologists, AAPG Special Volumes, A095,* 275–277.

Gunter, G. W., Finneran, J. M., Hartmann, D. J., & Miller, J. D. (1997). Early determination of reservoir flow units using an integrated petrophysical method. In *SPE annual technical conference and exhibition*. Society of Petroleum Engineers.

Hearn, C. L., Ebanks, W. J., Jr., Tye, R. S., & Ranganathan, V. (1984). Geological factors influencing reservoir performance of the Hartzog Draw Field, Wyoming. *Journal of Petroleum Technology, 36*(08), 1–335.

Hussien, T. M. H. (2014). *Formation evaluation of deep-water reservoirs in the 13A and 14A sequences of the Central Bredasdorp Basin, offshore South Africa*. The University of the Western Cape, South Africa student thesis. Retrieved March 24, 2020, from http://etd.uwc.ac.za/handle/11394/4876.

Jipa, D. C. (2012). Coarsening upward sedimentation in the Middle Pontian Dacian Basin, prograding shoreline or delta front? *Geo-Eco-Marina, 18,* 45.

Jungslager, E. H. (1999). Petroleum habitats of the Atlantic margin of South Africa. *Geological Society, London, Special Publications, 153,* 153–168.

Kolodzie Jr., S. (1980). Analysis of pore throat size and use of the Waxman-Smits equation to determine OOIP in Spindle Field, Colorado. In *SPE annual technical conference and exhibition*. Society of Petroleum Engineers.

Larue, D. K., & Legarre, H. (2004). Flow units, connectivity, and reservoir characterisation in a wave-dominated deltaic reservoir: Meren reservoir, Nigeria. *AAPG Bulletin, 88*(3), 303–324.

Levorsen, A. I., & Berry, F. A. (1967). *Geology of petroleum*. San Francisco: W.H. Freeman.

Magoba, M., & Opuwari, M. (2017). An interpretation of core and wireline logs for the Petrophysical evaluation of Upper Shallow Marine sandstone reservoirs of the Bredasdorp Basin, offshore South Africa. In *EGU general assembly conference abstracts* (Vol. 19, p. 14048).

Mahjour, S. K., Al-Askari, M. K. G., & Masihi, M. (2016). Identification of flow units using methods of Testerman statistical zonation, flow zone index, and cluster analysis in Tabnaak gas field. *Journal of Petroleum Exploration and Production Technology, 6*(4), 577–592.

Maseko, P. P. (2016). *Petrophysical evaluation and characterisation of sandstone reservoirs of the western Bredasdorp Basin, South Africa for well D-D1 and E-AP1*. The University of the Western Cape, South Africa. Student thesis. Retrieved March 24, 2020, from http://etd.uwc.ac.za/handle/11394/5181.

McMillan, I. K., Brink, G. J., Broad, D. S., & Maier, J. J. (1997). Late Mesozoic sedimentary basins off the south coast of South Africa. *Sedimentary Basins of the World*, *3*, 319–376.

Mirzaei-Paiaman, A., Ostadhassan, M., Rezaee, R., Saboorian-Jooybari, H., & Chen, Z. (2018). A new approach in petrophysical rock typing. *Journal of Petroleum Science and Engineering, 166,* 445–464.

Moradi, M., Moussavi-Harami, R., Mahboubi, A., Khanehbad, M., & Ghabeishavi, A. (2017). Rock typing using geological and petrophysical data in the Asmari reservoir, Aghajari Oilfield, SW Iran. *Journal of Petroleum Science and Engineering, 152,* 523–537.

Nabawy, B. S., & Al-Azazi, N. A. (2015). Reservoir zonation and discrimination using the routine core analyses data: The upper Jurassic Sab'atayn sandstones as a case study, Sab'atayn

basin, Yemen. *Arabian Journal of Geosciences, 8*(8), 5511–5530.

Nabawy, B. S., & Barakat, M. K. (2017). Formation evaluation using conventional and special core analyses: Belayim Formation as a case study, Gulf of Suez, Egypt. *Arabian Journal of Geosciences, 10*(2), 25.

Nabawy, B. S., Basal, A. M. K., Sarhan, M. A., & Safa, M. G. (2018). Reservoir zonation, rock typing and compartmentalisation of the Tortonian-Serravallian sequence, Temsah Gas Field, offshore Nile Delta, Egypt. *Marine and Petroleum Geology, 92,* 609–631.

Nabawy, B. S., & Geraud, Y. (2016). Impacts of pore- and petrofabrics, mineral composition and diagenetic history on the bulk thermal conductivity of sandstones. *Journal of African Earth Sciences, 115,* 48–62.

Newsham, K. E., & Rushing, J. A. (2001). An integrated workflow model to characterise unconventional gas resources: Part I-geological assessment and petrophysical evaluation. In *SPE annual technical conference and exhibition*. Society of Petroleum Engineers.

Ngejane, Z. (2014). *Seismic interpretation and 2D restoration of FA gas field, Bredasdorp Basin south coast of South Africa* (Thesis). The University of the Western Cape South Africa. Retrieved from, https://etd.uwc.ac.za/handle/11394/4656.

Ojongokpoko, H. M. (2006). *Porosity and permeability distribution in the deep marine play of the central Bredasdorp Basin, Block 9, offshore South Africa* (Thesis). The University of the Western Cape, South Africa. Retrieved from, http://etd.uwc.ac.za/handle/11394/2101.

Opuwari, M., Kaushalendra, B. T., & Momoh, A. (2019). Sandstone reservoir zonation using conventional core data: A case study of lower cretaceous sandstones, Orange Basin, South Africa. *Journal of African Earth Sciences*, *153*, 54–66.

Petroleum Agency of South Africa, PASA. (2003). *South African exploration opportunities*. Information brochure, South African Agency for Promotion of Petroleum.

Pittman, E. D. (1992). Relationship of porosity and permeability to various parameters derived from mercury injection-capillary pressure curves for sandstone. *AAPG Bulletin, 76*(2), 191–198.

Porras, J. C., Barbato, R., & Khazen, L. (1999). Reservoir flow units: A comparison between three different models in the Santa Barbara and Pirital fields, North Monagas Area, Eastern Venezuela Basin. In *Latin American and Caribbean petroleum engineering conference*. Society of Petroleum Engineers.

Porras, J. C., & Campos, O. (2001). Rock typing: A key Approach for Petrophysical characterization and definition of flow Units, Santa Barbara field, Eastern Venezuela Basin. In *SPE Latin American and Caribbean petroleum engineering conference*. Society of Petroleum Engineers.

Pranter, M. J., Hurley, N. F., & Davis, T. L. (2004). Sequence-stratigraphic, petrophysical, and multi-component seismic analysis of a shelf-margin reservoir: San Andres Formation (Permian), Vacuum field, New Mexico, United States. *The American Association of Petroleum Geologists, AAPG Memoir, 81,* 59–89.

Ramiah, K., Trivedi, K. B., & Opuwari, M. (2019). A 2D geomechanical model of an offshore gas field in the Bredasdorp Basin, South Africa. *Journal of Petroleum Exploration and Production Technology*, *9*(1), 207–222.

Reading, H. G. (2001). Clastic facies models, a personal perspective. *Bulletin of the Geological Society of Denmark, 48,* 101–115.

Riazi, Z. (2018). Application of integrated rock typing and flow units identification methods for an Iranian carbonate reservoir. *Journal of Petroleum Science and Engineering, 160,* 483–497.

Rider, M., & Rider, M. H. (2002). Facies, sequences and depositional environments from logs. In *The geological interpretation of well logs, 2nd ed. Sutherland, Scotland, Rider-French Consulting* (pp. 226–238).

Roux, J. (2000). The structural development of the southern Outeniqua Basin and Dias marginal fracture ridge. *Journal of African Earth Sciences, 31*(1), 64.

Rushing, J. A., Newsham, K. E., & Blasingame, T. A. (2008). Rock typing: Keys to understanding productivity in tight gas sands. In *SPE unconventional reservoirs conference*. Society of Petroleum Engineers.

Selley, R. C. (1998). *Elements of petroleum geology*. Houston, TX: Gulf Professional Publishing.

Selley, R. C., & Van der Spuy, D. (2016). *The oil and gas basins of Africa*. Episodes Vol. 39, No. 2, International Union of Geological Sciences. https://doi.org/10.18814/epiiugs/2016/v39i2/95786.

Shepherd, M. (2009). *Oil field production geology: AAPG Memoir 91* (Vol. 91). Tulsa, OK: AAPG.

Slatt, R. M., & Hopkins, G. L. (1990). Scaling geologic reservoir description to engineering needs. *Journal of Petroleum Technology, 42*(02), 202–210.

Stonecipher, S. A., Winn Jr, R. D., & Bishop, M. G. (1984). Diagenesis of the frontier formation, Moxa Arch: A function of sandstone geometry, texture and composition, and fluid flux: Part 3. Applications in exploration and production.

Tavakoli, V., Rahimpour-Bonab, H., & Esrafili-Dizaji, B. (2011). Diagenetic controlled reservoir quality of South Pars gas field, an integrated approach. *Comptes Rendus Geoscience, 343*(1), 55–71.

Tiab, D., & Donaldson, E. C. (2015). *Petrophysics: Theory and practice of measuring reservoir rock and fluid transport properties*. Houston, TX: Gulf Professional Publishing.

Turner, J. R., Grobbler, N., & Sontundu, S. (2000). Geological modelling of the Aptian and Albian sequences within Block 9, Bredasdorp Basin, offshore South Africa. *Journal of African Earth Sciences, 31*(1), 80.

Uguru, C. I., Onyeagoro, U. O., Lin, J., Okkerman, J., & Sikiru, I. O. (2005). Permeability prediction using genetic unit averages of flow zone indicators (FZIs) and neural networks. In *Nigeria annual international conference and exhibition*. Society of Petroleum Engineers.

Wood, M. (1995). Development potential is seen in Bredasdorp basin off South Africa. *Oil and Gas Journal, 93*(22), 54–58.

Xu, C., Heidari, Z., & Torres-Verdin, C. (2012). Rock classification in carbonate reservoirs based on static and dynamic petrophysical properties estimated from conventional well logs. In *SPE annual technical conference and exhibition*. Society of Petroleum Engineers.

Zhang, P., Lu, S., Li, J., Zhang, J., Xue, H., & Chen, C. (2018). Permeability evaluation on oil-window shale based on hydraulic flow unit: A new approach. *Advances in Geo-Energy Research, 2*(1), 1–13.